Transactions in Optics and Photonics
https://ojs.wiserpub.com/index.php/TOP/

Research Article

Optical Properties of Nanometer Epitaxial Nickel Oxide Films on $LiNbO_3$ Substrates

S. V. Averin*, **V. A. Luzanov, V. A. Zhitov, L. Yu. Zakharov, V. M. Kotov**

Fryazino Branch of the Kotel'nikov Institute of Radioengineering and Electronics of Russian Academy of Sciences, 141190, Square of Academician Vvedenski 1, Fryazino, Russia
E-mail: sva278@ire216.msk.su

Received: 6 March 2025; **Revised:** 30 April 2025; **Accepted:** 13 May 2025

Abstract: Nanometer epitaxial nickel oxide films have been successfully fabricated on $LiNbO_3$ substrates by magnetron sputtering. Optical properties of NiO films were studied in the wavelength range of 250-800 nm, and transmission and reflection spectra of these structures were simulated. The dispersion of the complex refractive index of the grown films was obtained, which ensures good agreement between the calculated and experimental transmission and reflection spectra. The band gap energy of NiO films was evaluated using Ultraviolet (UV)-visible spectroscopy. It is in the range of 3.57-3.59 eV. These studies allowed us to determine the thicknesses of the grown epitaxial films using optical methods and compare them with the results obtained based on the film growth rate and atomic force microscopy data.

Keywords: lithium niobate, nickel oxide, band gap, transmission spectrum, epitaxial film, atomic force microscopy, refractive index

1. Introduction

Active search for high-performance and cheap semiconductor materials for the UV and visible spectra has led to the study and practical application of a new class of semiconductors-metal oxides [1, 2]. Compared with GaN, AlGaN and Si metal oxide semiconductors provide low cost, ease of fabrication, and high responsivity in the UV region [3]. Nickel oxide is a promising candidate for the elaboration of various optoelectronic devices such as chemical sensors [4], optically transparent conductive films [5, 6], electrochromic coatings [7], solar cells [8], light-emitting diodes [9], and UV-radiation detectors [2, 10]. Since the light absorption coefficient of nickel oxide in the UV part of the spectrum is high, optical radiation is absorbed in a narrow near-surface region of the device [11]. For this reason, the active layers of optoelectronic devices are in the range of tens and hundreds of nanometers, and their thicknesses must be accurately controlled [2, 11].

Optical properties of NiO, such as spectral transmission and absorbance, absorption coefficient, band gap, refractive index, and extinction coefficient, are fundamental in understanding its influence on optoelectronic device characteristics [12]. It was observed previously that the substrates on which the NiO films are deposited significantly change the optical properties of the grown films, especially the band gap of NiO films [12]. Mostly, these were substrates made of sapphire, quartz glass, Si, and polymeric materials [1–3, 12–14]. In this paper, we present for the first time the results of experimental

DOI:

studies of the optical properties of epitaxial nanometer nickel oxide films grown on lithium niobate substrates. Lithium niobate is a traditional material for use in optical modulators, surface acoustic wave devices, laser frequency doubling, optical switches, nonlinear optics, optical waveguides, electro-optical, acousto-optic, and acousto-electronic devices and the optical properties of nickel oxide films on $LiNbO_3$ substrate is of undoubted interest both for various physical studies and for elaboration of optoelectronic devices based on them. In addition, as our studies have shown, a small mismatch of crystal lattices allows for obtaining structurally perfect thin layers of NiO on $LiNbO_3$ substrates [15].

2. Experimental details

Single-crystal (0001) $LiNbO_3$ was used as a substrate material for growing nickel oxide films. A modified vacuum cathode sputtering unit, A550 VZK (Leybold Heraeus GmbH), equipped with a magnetic system, was used for the deposition of nickel oxide films. A nickel target with a diameter of 100 mm was used in the work. After the experiments, optimal conditions for the deposition of NiO films were found to achieve their high crystalline perfection [15, 16]. Sputtering was performed at a direct current of 200 mA. The gas pressure during discharge was 6×10^{-3} Torr with equal percentage concentrations of oxygen and argon. The substrate was preheated to 400 °C. The deposition rate under these conditions was 800 nm per hour. The details of the deposition process have been presented at length in [15]. In our experiments, the thickness of the deposited films was in the range of 50-500 nm, which was determined by sputtering time, refined by the data obtained after optical transmission processing, and also measured by atomic force microscopy. A SPECORD Ultraviolet-Visible (UV-VIS) spectrophotometer was used to record the spectra of the samples.

3. Results and discussion

The surface of the initial $LiNbO_3$ substrates and NiO films grown on them was studied using a Smart Scanning Probe Microscope (SPM) atomic force microscope (AIST-NT). The estimated root-mean-square height of irregularities, Root Mean Square (RMS) = 0.25 nm, for the initial $LiNbO_3$ substrate was determined from image analysis using the Gwyddion program. Thus, the used substrates are of very high quality and practically do not contribute to the surface morphology of the grown films. As a result, for the grown $NiO/LiNbO_3$ heterostructure with a NiO epitaxial layer thickness of 50 nm, the estimated root-mean-square height of irregularities over an area of $1.5 \times 1.5\ \mu m^2$ is RMS = 1.73 nm. With increasing thickness of the NiO film, the root-mean-square height of the epitaxial layer irregularities increases through the accumulation of defects due to ion bombardment of the surface. Thus, with a film thickness of 200 nm, this amount is already equal to RMS = 2.97 nm. For comparison, authors have reported the surface roughness of RMS = 5 nm for a NiO film with a thickness of 100 nm after thermal spraying of NiO powder [2]. The RMS = 9.87 nm was measured in a nanostructured NiO film on Si (100) substrate using a sol-gel spin coating technique [17].

The optical transmission and reflection of pure $LiNbO_3$ substrates and fabricated $NiO/LiNbO_3$ heterostructures were studied in the wavelength range of 250-800 nm. Figure 1 (curves 1-4) shows the experimental transmission spectra of the heterostructures (NiO film/$LiNbO_3$ substrate) with a NiO layer of different thicknesses. For the sake of comparison, the transmission spectra of two structures with fused quartz as a substrate (samples # 9 and # 10) were also investigated. These spectra are given in Figure 2. There is a small decrease in the optical transmittance of the NiO film with increasing film thickness, which might be due to free-carrier absorption corresponding to an increase in the film conductivity [18, 19]. In addition, Figure 2 shows a slight shift in the absorption edge towards higher wavelengths, suggesting a decrease in the energy band gap of NiO with increasing film thickness. This red shift could be related to the coloration effect on the films [20].

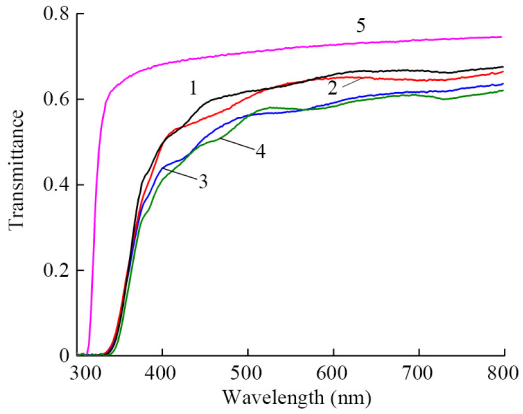

Figure 1. Experimental optical transmittance as a function of wavelength: 1-4-NiO/$LiNbO_3$ heterostructures with NiO thickness d: 1-sample # 5, $d = 360$ nm; 2-sample # 3, $d = 320$ nm; 3-sample # 2, $d = 380$ nm; 4-sample # 7, $d = 525$ nm; 5-pure $LiNbO_3$ substrate

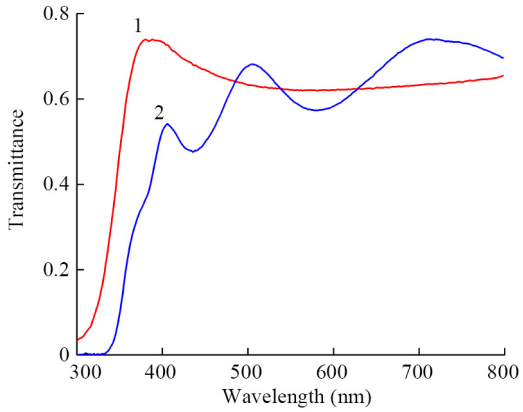

Figure 2. Experimental transmission spectra of NiO/SiO_2 substrate structures: 1-sample # 9, NiO film thickness $d = 73$ nm, 2-sample # 10, NiO film thickness $d = 335$ nm

It is evident that the optical transmission of NiO films in the wavelength range of 450-800 nm is ~60%, which is in good agreement with the light transmission in NiO films grown in other studies, for example, on clean glass [2]. The absorption edge of NiO films is at a wavelength of ~340 nm. Before deposition of NiO films, the optical properties of the $LiNbO_3$ substrates themselves were also studied, Figure 1, curve 5. The $LiNbO_3$ substrate has an absorption edge at a wavelength of ~310 nm and effectively transmits light in the longer-wavelength region. Consequently, when illuminated from the substrate side, it can be suitable to study the optical properties of materials (and devices based on them), the band gap of which falls in the wavelength range exceeding ~310 nm. In particular, this makes it possible to create on the NiO/$LiNbO_3$ heterostructure a narrow-band detector with the photoresponse limited to the range of wavelengths 310-340 nm. This detector is solar blind and, allows us to fix biologically hazardous solar radiation in the wavelength range from 310 to 340 nm [11]. It is also well known that a narrow-band photodetector improves the dynamic range and noise immunity of information and measurement systems [11].

Comparing the experimental transmission spectrum of the initial $LiNbO_3$ substrate (curve 5 in Figure 1) with the experimental transmission spectra of the samples with NiO/$LiNbO_3$ heterostructures (Figure 1, curves 1-4), we may see some minute oscillations in the transmission spectra of the samples 1-4 at the wavelength longer than ~380 nm. These oscillations are associated with interference in the layered NiO/$LiNbO_3$ structure. This assumption is confirmed by the observations of other researchers for the NiO films grown on different substrates [12, 17]. Since light passes through two semitransparent surfaces, it is partially reflected from each of them and thus results in reabsorption and interference

processes, which are usually considered as Fabry-Perot oscillations [12, 17]. Modeling of transmission/reflectance spectra confirms this assumption.

To calculate the transmittance and reflection spectra of the multilayer heteroepitaxial structures NiO/$LiNbO_3$ and NiO/SiO_2, we have applied the 2×2 matrix method [21]. It is assumed that each layer of the structure is a linear, homogeneous, and isotropic medium, described by the complex refractive index N and its thickness d. The optical properties are uniform within each layer of the structure and change abruptly at the sharp interfaces between layers. The reflection and transmission coefficients of the layered structure are expressed through the elements of the scattering matrix. The scattering matrix S connects the complex amplitudes of the electric field E_0 in the external medium and that of E_2 in the substrate in the plane directly adjacent to the interface with the NiO layer, i.e., $E_0 = S \cdot E_2$.

The scattering matrix can be represented as a product of the interface and layer matrices I and L:

$$S = I_{01} \times L_1 \times I_{12}. \tag{1}$$

The interface matrix I is expressed in terms of the Fresnel reflection and transmission coefficients of the interface, which, in turn, are determined by the complex refractive indices of the adjacent media, the angle φ of light incidence, and by polarization p-parallel or s-perpendicular to the plane of incidence. The layer matrix L_1 is expressed in terms of the phase shift β of a plane wave λ incident at an angle φ and passing through a NiO layer of thickness d_1 with the complex refractive index N_1:

$$\beta = (2\pi d_1 N_1/\lambda)\cos(\varphi). \tag{2}$$

The overall reflection and transmission coefficients of the layered structure are expressed in terms of the elements of the scattering matrix S:

$$R = (S_{21}/S_{11}), \tag{3}$$

$$T = (1/S_{11}). \tag{4}$$

By the experimental conditions, the angle of incidence for the calculation was taken to be zero, and the contributions of p-and s-polarizations were assumed to be the same.

Since the $LiNbO_3$ substrate thickness is ~ 440 μm and significantly exceeds the coherence length (~ 80 μm), only the interference in the NiO film was taken into account when modeling the transmission of the NiO/$LiNbO_3$ structures. Therefore, the matrix method was used to calculate the transmission of light incident from air and passing through the NiO film into the $LiNbO_3$ half-space. In this case, since there is almost no light absorption in $LiNbO_3$ in the modeled wavelength range, the obtained value was multiplied by the transmittance of the $LiNbO_3$/air interface. When modeling the reflection, the matrix method was used to calculate the reflection of light incident from the air onto the NiO/$LiNbO_3$ half-space structure.

Modeling of the transmission/reflection spectra also allowed us to obtain the dispersion of the refractive index of the grown NiO films. Since the surface of the $LiNbO_3$ substrate has the orientation (0001), the dispersion of the refractive index of the ordinary ray $n^2_{(0)}$ was used to model the transmission of the structures under study, which, in accordance with the Sellmeier equation, is written [22]:

$$n^2_{(0)} - 1 = \frac{2.6734\lambda^2}{\lambda^2 - 0.01764} + \frac{1.2290\lambda^2}{\lambda^2 - 0.05914} + \frac{12.614\lambda^2}{\lambda^2 - 474.60}. \quad (5)$$

In the case of the fused silica substrate, we used the refractive index dispersion of SiO_2.

Taking into account the insignificant value of interference oscillations observed in the transmission spectra of $NiO/LiNbO_3$ samples (Figure 1), when modeling the transmission we used the dispersion of the real part of the refractive index of NiO, starting from the dispersion of $LiNbO_3$, and used slightly lower values of the refractive index. In the modeling process we used, as starting values, the film thicknesses based on the growth time under the assumption of a constant NiO deposition rate during magnetron sputtering. To achieve maximum compliance with the position of interference oscillations on the experimental and calculated curves, we varied the dispersion of the real part of the refractive index of the NiO layer and its thickness. At the same time, the introduction of the imaginary part k (extinction coefficient) of the refractive index made it possible to match the calculated transmission levels with the experimental values. The dispersion of the imaginary part k of the refractive index of NiO can be obtained using $k = \alpha\lambda/4\pi$ [23] by determining the dependence of the absorption coefficient α on the wavelength λ from the experimental curves. Then, if T_{sample} is the transmittance of the whole sample (NiO film/substrate), and T_{sub} is the transmittance of the substrate itself, and using d-the thickness of the NiO layer, corrected in the modeling process, we can write:

$$T(\lambda) \sim \exp(-\alpha(\lambda)d) = T_{\text{sample}}/T_{\text{sub}}, \quad (6)$$

$$\alpha(\lambda) = -\ln T(\lambda)/d, \quad (7)$$

where λ is the radiation wavelength, $T(\lambda)$ is the transmission of the NiO layer itself. Figure 3 shows the absorption coefficients $\alpha(\lambda)$ for the films under investigation (samples # # 2, 5, 7, 10) as a function of the radiation wavelength. The absorption coefficients grow exponentially with decreasing wavelength, reaching $\alpha = 2 \times 10^5$ cm^{-1} at a wavelength of $\sim$ 340 nm and in good agreement with previously obtained values for films deposited on glass and polymer substrates [12].

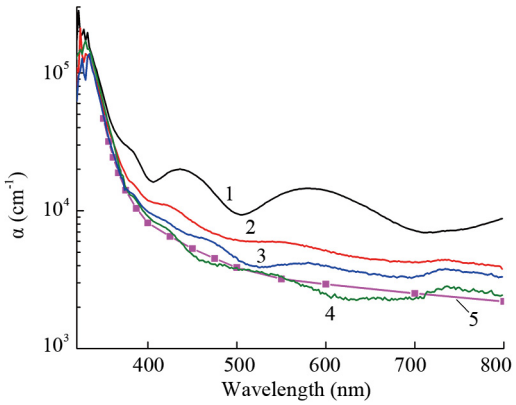

Figure 3. Absorption coefficients of NiO films as a function of the wavelength: 1-sample # 10, SiO_2 substrate; 2-sample # 2, $LiNbO_3$ substrate; 3-sample # 7, $LiNbO_3$ substrate; 4-sample # 5, $LiNbO_3$ substrate; 5-model experiment for the sample # 5

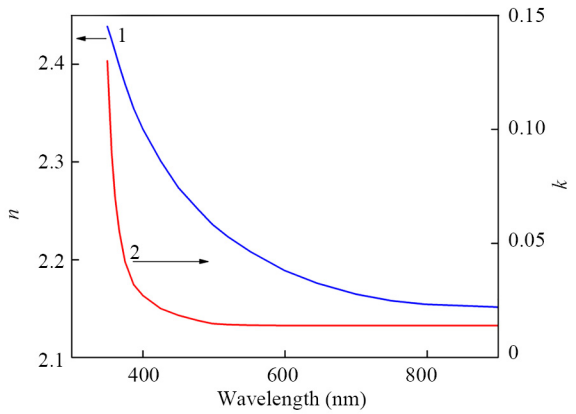

Figure 4. Dispersion of refractive index n and extinction coefficient k for the sample # 5 (NiO film 360 nm/$LiNbO_3$ substrate)-the simulation results

By approximating the dependence $\alpha(\lambda)$ for sample # 5 with minimal absorption in the region of transparency (curve 5 in Figure 3), we have determined the imaginary part of the dispersion of refractive index k for this sample. The resulting dispersion of refractive index and extinction coefficient of the NiO film for sample # 5 is shown in Figure 4. A sharp increase in both refractive index and extinction coefficient is observed in the region of strong absorption of NiO corresponding to the edge of the NiO band gap at a wavelength of ~ 340 nm and is usually associated with anomalous dispersion [24, 25]. In the region of optical transparency, the absorption in NiO is small $(k \sim 0.014)$ and both n and k decrease exponentially, which corresponds to normal dispersion [12, 24, 25]. The values of n and k for sample # 5 are equal to 2.44 and 0.13, respectively, at wavelengths shorter than 380 nm and are in good agreement with the data for the NiO films deposited on quartz glasses and polymeric materials [12]. For the rest of our samples, the best agreement between experimental and calculated data is ensured by introducing a slight additional optical absorption Δk, i.e., by increasing the imaginary part k of the complex refractive index for the NiO layer $(\Delta k \sim 0.004 - 0.015$, see Table 1). This is illustrated in Figures 5 and 6.

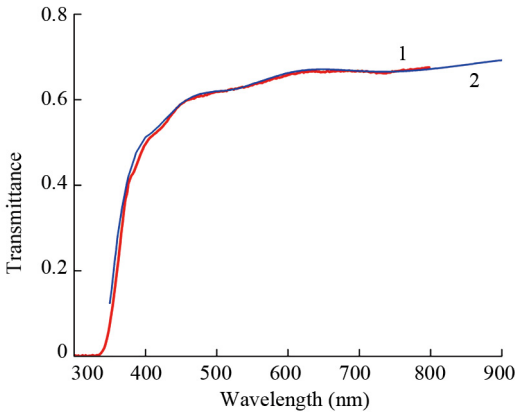

Figure 5. Transmission spectra of sample # 5 (NiO film 360 nm/$LiNbO_3$ substrate): 1-experiment, 2-calculated dependence at $\Delta k = 0$

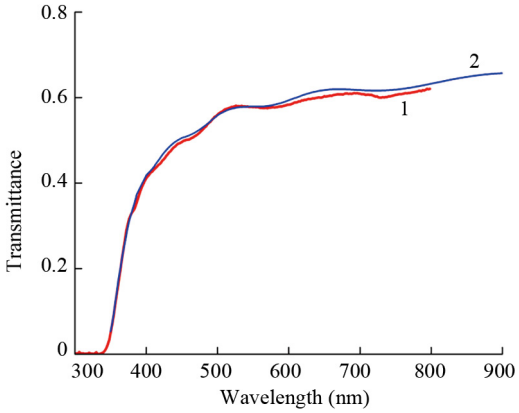

Figure 6. Transmission spectra of sample # 7 (NiO film 525 nm/$LiNbO_3$ substrate): 1-experiment, 2-calculated dependence at $\Delta k = 0.004$

Table 1. Parameters of the NiO films

Sample	NiO film thickness, nm (modeling)	NiO film thickness, nm (based on the growth rate)	Eg, eV	Δk
# 2 (NiO / $LiNbO_3$)	380	400	3.59	0.010
# 3 (NiO / $LiNbO_3$)	320	300	3.58	0.004
# 5 (NiO / LiNbO)	360	350	3.59	0
# 7 (NiO / $LiNbO_3$)	525	500	3.57	0.004
# 8 (NiO / $LiNbO_3$)	200	200		
# 9 (NiO / SiO_2)	73	100	3.58	
# 10 (NiO/SiO2)	335	300	3.58	0.015

The optical properties of the NiO films grown on fused silica were also investigated, Figure 2. It turned out that the dispersion of the refractive index of NiO found for NiO/$LiNbO_3$ structures is also suitable for films grown on fused silica. The transmission and reflection simulation for the sample # 10-NiO/SiO_2 is shown in Figures 7, 8. Since NiO films on fused silica exhibit somewhat higher optical absorption in the transparency region compared to the samples on $LiNbO_3$ substrate, an additional absorption of the complex refractive index of the NiO layer must be added to match the calculated and experimental transmission levels, and for the sample # 10, $\Delta k \sim 0.015$. Note that in the case of the samples on $LiNbO_3$ substrate, this value is noticeably smaller and lies in the range of 0.004-0.01.

It is interesting to compare the thicknesses of our epitaxial NiO films determined by different methods. For this purpose, we used sample # 8, in which, using lift-off photolithography, a 200 nm thick nickel oxide film was deposited only on part of its surface. The sharp step between the $LiNbO_3$ substrate and the deposited NiO film allowed us to measure the thickness of the NiO film using atomic force microscopy. Measurements were performed at three points along the line of the sharp transition between the substrate and the deposited NiO and showed that the film thickness for this sample is within 200-230 nm, which is in good agreement with the results based on the film growth rate and those obtained by optical measurements. However, it is worth noting that optical methods make it possible to determine the thickness of the grown film without destroying the structure of its surface. The results of the investigations of heterostructures NiO/$LiNbO_3$ and NiO/SiO_2 are summarized in Table 1.

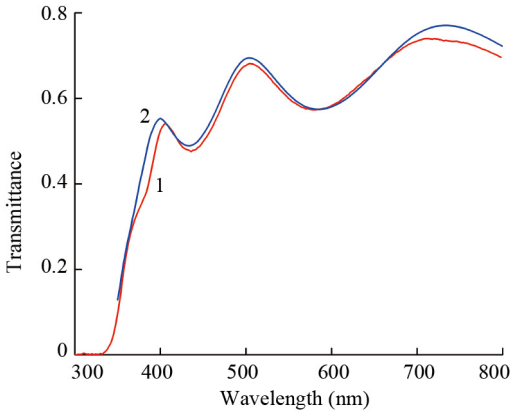

Figure 7. Transmission spectra of sample # 10 (NiO film 335 nm/SiO_2 substrate): 1-experiment, 2-calculated dependence at $\Delta k = 0.015$

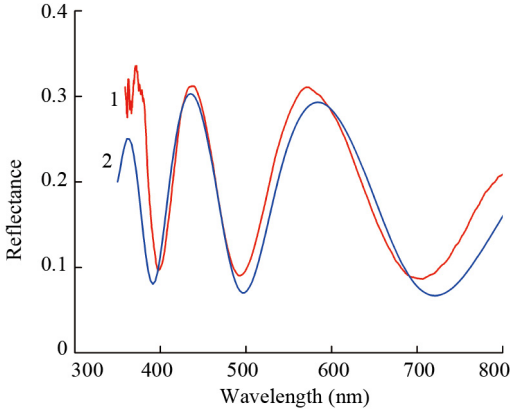

Figure 8. Reflectance spectra of sample # 10 (NiO film 335 nm/SiO_2 substrate): 1-experiment, 2-calculated dependence, $\Delta k = 0.015$

To calculate the band gap in the NiO films under study, the Tauc equation [26] was used:

$$(\alpha hv)^2 = A\,(hv - E_g)\,, \tag{8}$$

where hv is the photon energy, E_g is the band gap, A is a constant, and α is the absorption coefficient. By plotting the graph $(\alpha hv)^2 vs(hv)$ (Figures 9, 10) and extrapolating the linear section to the intersection point with the hv axis, we can determine E_g of the deposited films.

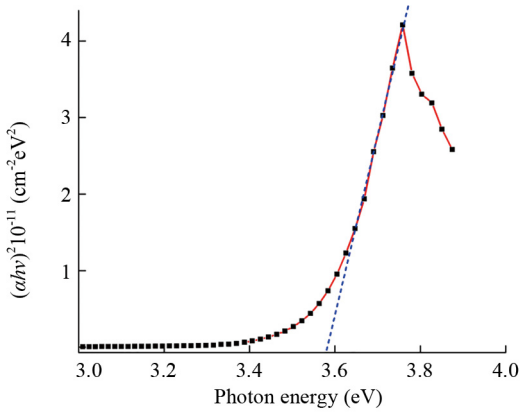

Figure 9. The Tauc plot, sample # 5 (NiO film 360 nm/$LiNbO_3$ substrate), $E_g = 3.59$ eV

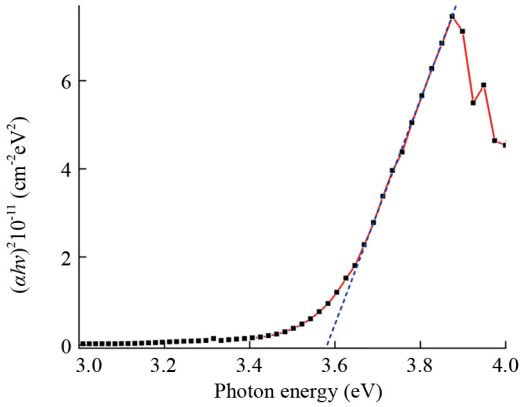

Figure 10. The Tauc plot, sample # 10 (NiO film 335 nm/SiO_2 substrate), $E_g = 3.59$ eV

The absorption edge values found for all structures under study are in the range of 3.57-3.59 eV. The band gap width did not change with increasing thickness of the NiO films grown on $LiNbO_3$ substrates, which indicates a high degree of its homogeneity. For comparison, the optical band gap energy of NiO deposited on glass and acetate plastic substrates was 3.5 eV, that of on sapphire is 4.2 eV, and that of on CaF is 4.5 eV [12]. In [10], the authors reported the absorption edge for the NiO/ZnO heterojunction grown on a glass substrate as 3.4 eV. For NiO nanomaterial produced by laser ablation in water on silicon substrate, the band gap varied from 3.6 to 3.8 eV depending on the laser energy [27]. Thus, different substrates alter the energy band gap of NiO, which is in a relatively wide range and, as a consequence, will strongly influence the optical properties of the final optoelectronic devices.

4. Conclusion

The nanometer NiO films were successfully grown on $LiNbO_3$ substrates. Atomic force microscopy confirms the smoothness of the films. The experimental optical transmission and reflection of initial $LiNbO_3$ substrates and fabricated NiO/$LiNbO_3$ heterostructures were studied in the wavelength range of 250-800 nm. Transmission and reflection spectra of NiO/$LiNbO_3$ structures were simulated. The dispersion of the complex refractive index of the grown films was obtained, which ensures good agreement between the calculated and experimental transmission and reflection curves. The dispersion of the refractive index of NiO is also well suited for films grown on fused quartz. It was found that NiO films on fused quartz have slightly higher absorption as compared to the samples on $LiNbO_3$ substrates. Modeling of transmission

spectra of $NiO/LiNbO_3$ heterostructures made it possible to determine the thickness of NiO semiconductor layers without destroying the surface structure. Active layer thicknesses of the grown heterostructures were determined by three different methods and are in good agreement with each other. The band gap energy of NiO films was evaluated using UV-visible spectroscopy. It was equal to 3.57-3.59 eV.

Funding

This work was carried out within the framework of the state assignment of the Institute of Radioengineering and Electronics of Russian academy of sciences (IRE RAS).

Author contributions

Averin S. V.-project administration, written the first draft of the manuscript, formal analysis, conceptualization, review & editing.

Luzanov V. A.-preparation of samples, review & editing.

Zhitov V. A.-measurements, review & editing, validation, supervision.

Zakharov L. Yu.-measurements, investigation, resources, validation, review & editing.

Kotov V. M.-supervision, review & editing.

All authors read and approved the final manuscript.

Data availability

The datasets generated during and/or analyzed during the current study are available from the corresponding author on reasonable request.

Conflict of interest

The authors declare no competing interests.

References

[1] Gupta R, Hendi AA, Cavas M, Al-Ghamdi A, Al-Hartomy OA, Aloraini RH, et al. Improvement of photoresponse properties of NiO/p-Si photodiodes by copper dopant. *Physica E Low-dimensional Systems and Nanostructures*. 2014; 56: 288-295. Available from: https://doi.org/10.1016/j.physe.2013.09.014.

[2] Choi JM, Im S. Ultraviolet enhanced Si-photodetector using *p*-NiO films. *Aplied Surface Science*. 2005; 244(1-4): 435-438. Available from: https://doi.org/10.1016/j.apsusc.2004.09.152.

[3] Balakarthikeyan R, Santhanam A, Anandhi R, Vinoth S, Al-Baradi AM, Alrowaili ZA, et al. Fabrication of nanostructured NiO and NiO: Cu thin films for high-performance ultraviolet photodetector. *Optic Materials*. 2021; 120: 11387. Available from: https://doi.org/10.1016/j.optmat.2021.111387.

[4] Steinebach H, Kannan S, Rieth L, Solzbacher F. H_2 gas sensor performance of NiO at high temperatures in gas mixtures. *Sensors and Actuators B: Chemical*. 2010; 151 (1): 162-168. Available from: https://doi.org/10.1016/j.snb.2010.09.027.

[5] Sasi B, Gopchandran KG, Manoj PK, Koshy P, Prabhakara Rao P, Vaidyan VK. Preparation of transparent and semiconducting NiO films. *Vacuum*. 2003; 68(2): 149-154. Available from: https://doi.org/10.1016/S0042-207X(02)00299-3.

[6] Sato H, Minami T, Takata S, Yamada T. Transparent conducting *p*-type NiO thin films prepared by magnetron sputtering. *Thin Solid Films*. 1993; 236(1-2): 27-31. Available from: https://doi.org/10.1016/0040-6090(93)90636-4.

[7] Lou XC, Zhao XJ, He X. Boron doping effects in electrochromic properties of NiO films prepared by sol-gel. *Solar Energy*. 2009; 83(12): 2103-2108. Available from: https://doi.org/10.1016/j.solener.2009.06.020.

[8] Bandara J, Weerasinghe H. Solid-state dye-sensitized solar cell with p-type NiO as a hole collector. *Solar Energy Materials and Solar Cells*. 2005; 85(3):385-390. Available from: https://doi.org/10.1016/j.solmat.2004.05.010.

[9] Park SW, Choi JM, Kim E, Im S. Inverted top-emitting organic light-emitting diodes using transparent conductive NiO electrode. *Applied Surface Science*. 2005; 244(1-4): 439-443. Available from: https://doi.org/10.1016/j.apsusc.2004.10.099.

[10] Tsai SY, Hon MH, Lu YM. Fabrication of transparent *p*-NiO/n-ZnO heterojunction devices for ultraviolet photodetectors. *Solid-State Electronics*. 2011; 63(1): 37-41. Avilable from: https://doi.org/10.1016/j.sse.2011.04.019.

[11] Blank TV, Gol'dberg YA. Semiconductor photoelectric converters for the ultraviolet region of the spectrum. *Semiconductors*. 2003; 37(9): 999-1030. Available from: https://doi.org/10.1134/1.1610111.

[12] Manjumatha KN, Paul Sh. Investigation of optical properties of nickel oxide thin films deposited on different substrates. *Applied Surface Science*. 2015; 352: 10-15. Available from: https://doi.org/10.1016/j.apsusc.2015.03.092.

[13] Uchida K, Yoshida K, Zhang D, Koizumi A, Nozaki S. High-quality single crystalline NiO with twin phases grown on sapphire substrate by metalorganic vapor phase epitaxy. *AIP Advances*. 2012; 2(4): 042154. Available from: https://doi.org/10.1063/1.4769082.

[14] Ryu HW, Choi GP, Lee WS, Park JS. Preferred orientations of NiO thin films prepared by RF magnetron sputtering. *Journal of Materials Science*. 2004; 39(13): 4375-4377. Available from: https://doi.org/10.1023/B:JMSC.0000033431.52659.e5.

[15] Luzanov VA. Growth of thin epitaxial NiO films on $LiNbO_3$ substrates. *Journal of Communications Technology and Electronics*. 2020; 65(12): 1422-1424. Available from: https://doi.org/10.1134/S106422692011011X.

[16] Averin SV, Luzanov VA, Zhitov VA, Zaharov LY, Kotov VM, Temiryazeva MP, et al. Nikel oxide epitaxial films and diode structures based on them. *Journal of Communications Technology and Electronics*. 2024; 69(9): 908-923. Available from: https://doi.org/10.31857/S0033849424090124.

[17] Ahmed AA, Hashim MR, Abdalrheem R, Rashid M. High-performance multicolor metal-semiconductor-metal Si photodetector enhanced by nanostructured NiO thin film. *Journal of Alloys and Compounds*. 2019; 798: 300-310. Available from: https://doi.org/10.1016/j.jallcom.2019.05.286.

[18] Svensson JSEM, Granqvist CG. Modulated transmittance and reflectance in crystalline electrochromic WO_3 films: Theoretical limits. *Applied Physics Letters*. 1984; 45(8): 828-830. Available from: https://doi.org/10.1063/1.95415.

[19] Al-Ghamdi AA, Abdel-wahab MS, Farghali AA, Hasan PMZ. Structural, optical and photo-catalytic activity of nanocrystalline NiO thin films. *Materials Research Bulletin*. 2016; 75: 71-77. Available from: https://doi.org/10.1016/j.materresbull.2015.11.027.

[20] Usha KS, Sivakumar R, Sanjeeviraja C. Optical constants and dispersion energy parameters of NiO thin films prepared by radio frequency magnetron sputtering technique. *Journal of Applied Physics*. 2013; 114(12): 123501. Available from: https://doi.org/10.1063/1.4821966.

[21] Azzam RMA, Bashara NM. *Ellipsometry and Polarized Light*. Netherlands: North-Holland Publishing Company; 1977.

[22] Zelmon DE, Small DL, Jundt D. Infrared corrected Sellmeier coefficients for congruently grown lithium niobate and 5 mol.% magnesium oxide-doped lithium niobate. *Journal of the Optical Society of America B*. 1997; 14(12): 3319-3322. Available from: https://doi.org/10.1364/JOSAB.14.003319.

[23] Tripathi SK, Gupta S, Mustafa FI, Goyal N, Saini GSS. Laser induced changes on a-Ga50Se50 thin films. *Journal of Physics D: Applied Physics*. 2009: 42(18): 185404. Available from: https://doi.org/10.1088/0022-3727/42/18/185404.

[24] Yu PY, Cardona M. *Fundamentals of Semiconductors, Physics and Material Properties*. 3rd ed. Heidelberg: Springer; 1997. Available from: https://doi.org/10.1007/b137661.

[25] Adachi S. *Optical Constants of Crystalline and Amorphous Semiconductors: Numerical Data and Graphical Information*. Heidelberg: Springer; 1999.

[26] Tauc J. Optical properties and electronic structure of amorphous Ge and Si. *Materials Research Bulletin*. 1968; 3(1): 37-46. Available from: https://doi.org/10.1016/0025-5408(68)90023-8.

[27] Khashan KS, Saimon JA, Hadi AA, Mahdi RO. Influence of laser energy on the optoelectronic properties of NiO/Si heterojunction. *Journal of Physics: Conference Series*. 2021; 1795: 012026. Available from: https://doi.org/10.1088/1742-6596/1795/1/012026.